^{40}Ca+ ^{40}Ca reaction at E_{lab}=35 MeV/nucleon: Filters and signatures to distinguish nearly central from peripheral collisions

P. Pawłowski,[1] J. Brzychczyk,[1] D. Benchekrovn,[2] E. Bisquer,[2] P. Burzyński,[1] A. Chabane,[3] M. Charvet,[3] B. Cheynis,[2] A. J. Cole,[3] A. Demeyer,[2] P. Desesquelles,[3] W. Gawlikowicz,[1] E. Gerlic,[2] A. Giorni,[3] K. Grotowski,[1,4] D. Guinet,[2] P. Hachaj,[1] D. Heuer,[3] P. Lautesse,[2] L. Lebreton,[2] A. Lleres,[3] S. Micek,[1] R. Płaneta,[1] Z. Sosin,[1] M. Stern,[2] L. Vagneron,[2] J. B. Viano,[3] and A. Wieloch[1]

[1]*M. Smoluchowski Institute of Physics, Jagellonian University, Reymonta 4, 30-059 Cracow, Poland*

[2]*Institut de Physique Nucléaire de Lyon, IN2P3-CNRS/Université Claude Bernard 43, Boulevard du 11 Novembre 1918, F-69622 Villeurbanne Cedex, France*

[3]*Institut des Sciences Nucléaires de Grenoble, IN2P3-CNRS/Université Joseph Fourier 53, Avenue des Martyrs, F-38046 Grenoble Cedex, France*

[4]*H. Niewodniczański Institute of Nuclear Physics, Radzikowskiego 152, 31-342 Cracow, Poland*

(Received 26 April 1995; revised manuscript received 14 March 1996)

Multifragment emission of charged particles from the ^{40}Ca + ^{40}Ca reaction at 35 MeV/nucleon has been investigated. Multiplicity as well as event shape filters were used to distinguish nearly central from peripheral collisions. A correlation between higher multiplicities and random events from two reactions occurring in one beam burst is discussed. Signatures of different reaction scenarios are investigated using simulation techniques. [S0556-2813(96)50307-9]

PACS number(s): 25.70.Gh, 25.70.Lm, 25.70.Pq

Multifragmentation of nuclei has been studied in many experimental and theoretical works [1–4]. It is expected that such phenomena can be used for studying thermodynamic properties of hot nuclear systems (nuclear matter) [2].

In the case of a heavy-ion reaction, one may expect multifragmentation of a composite system created in a nearly central collision (NCC) but also multifragmentation of one or both of the two highly excited fragments produced in more peripheral deep inelastic collisions (DIC), which dominate the reaction picture at intermediate energies (see, e.g., [5,6]). In order to compare experimental data with predictions of various theoretical models it is thus necessary to separate events corresponding to different impact parameters. Special conditions imposed event by event on the data are used for that purpose. The most popular one is the high multiplicity threshold, as there exists a simple relation between multiplicity and impact parameter (angular momentum) [7]. Other observables used for construction of filters are centrality [8], midrapidity charge [9], average parallel velocity [10], total transverse momentum [10], second moment of the charge distribution [1], the total detected charge [11], and the momentum tensor (see [10] and references therein). Comparison of different filters was made in [10] for the asymmetric ^{40}Ar + ^{27}Al system.

In this work we discuss the problem of separation of NCC's in the ^{40}Ca + ^{40}Ca reaction at 35 MeV/nucleon. The multifragment emission from this reaction has been investigated at SARA (Hagel *et al.* [1]), using the AMPHORA detector system [12]. It consisted of 140 CsI detectors of which 92 detectors included fast plastic scintillators on the front faces. These latter detectors were used to identify intermediate mass fragments (IMF's), albeit with relatively high energy thresholds (about 7 MeV/nucleon). Detection of heavier charged particles provides more information for analysis of the reaction mechanism. We therefore decided to repeat the measurements with the upgraded AMPHORA. In the present experiment 30 gas ionization chambers were placed in front of the CsI detectors lowering energy thresholds to about 1 MeV/nucleon [13]. This installation was made for two AMPHORA rings, at angles 31.2 and 46.6 degrees, for which computer simulations suggested a large cross section for intermediate mass fragments. The AMPHORA detectors cover about 80% of 4π. No on-line triggers were applied and low beam intensity was used throughout the run in order to reduce the rate of accidental events. Windows were set on time spectra to clean data from accidental coincidences. For analysis we used only events in which the total detected charge Z_{tot} was at least 85% of the charge, available in the entrance reaction channel Z_0 but smaller then 41. Elastic scattering of ^{4}He, ^{12}C, ^{16}O, and ^{20}Ne ions at four different energies was used for the IMF energy calibration. A more detailed description of the experimental procedure and results of the present experiment will be given in a forthcoming paper. Experimental results of this paper agree generally with the data published in [1]. They contain, as expected, much broader energy spectra of IMF's (see Fig. 1).

As a first step of data processing the high multiplicity threshold was applied for elimination of the DIC events. In order to evaluate the efficiency of this filter, model calculations have been performed using a Monte Carlo event generator [14]. Here the interaction potential of colliding ions is computed. For smaller impact parameters, when the system is trapped in a potential pocket a composite system is formed. It may decay either by prompt or by sequential multifragmentation [15]. Otherwise, the collision is treated as a DIC [16,6], with a formation and subsequent deexcitation of two hot Ca-like fragments. For the larger angular momenta contributing to fusion the fission channel is favored. For comparison with data, the solid lines in Fig. 1 [see also Figs.

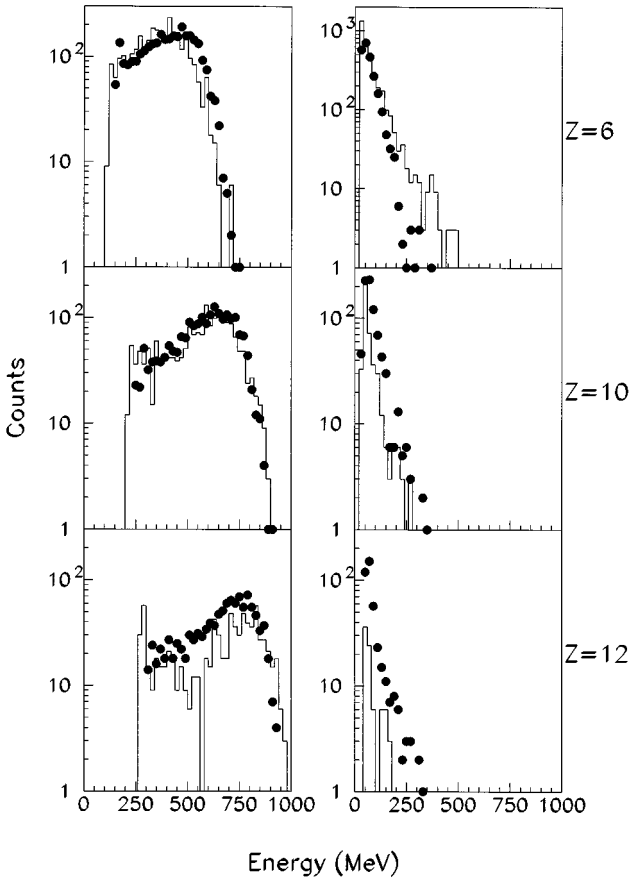

FIG. 1. Measured energy distributions of $Z=6$,10, and 12 fragments at angles 7.8 and 46.6 degrees. Histograms represent predictions of the Monte Carlo event generator.

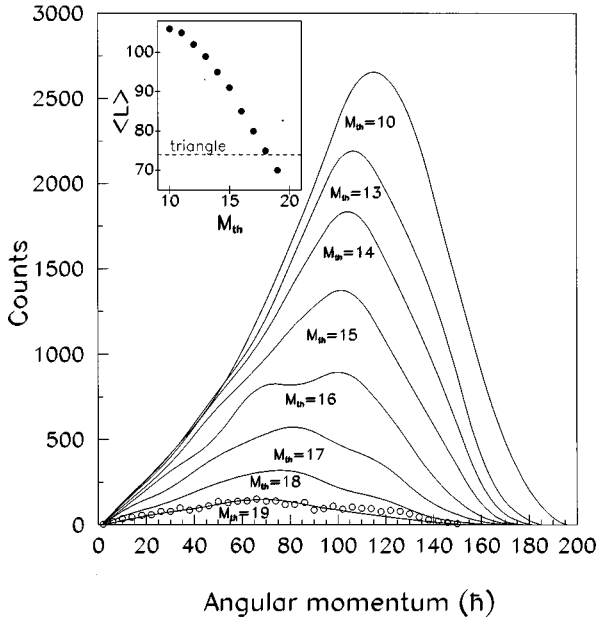

FIG. 2. Number of events vs angular momentum, predicted by the event generator, for different values of multiplicity thresholds M_{th}. Circles indicate an angular momentum window for $M_{th}=16$ plus restriction to events located inside the triangle $(a,b)(1,0)$ (Fig. 4). $33<Z_{tot}<41$ was required for all the multiplicity filters. The $\langle L\rangle$ vs M_{th} plot is given in the inset. The horizontal line corresponds to the ''triangle'' filter.

6(a) and 6(c)] show predictions of the event generator. In each case the influence of the AMPHORA detector system and of respective filters was taken into account [17].

Figure 2 presents distribution of events from ^{40}Ca + ^{40}Ca collisions vs angular momentum L, predicted by the event generator for different multiplicity thresholds M_{th}. As one can see, the angular momentum windows shift toward smaller L values with increasing M_{th}, and for $M_{th}=19$ the angular momentum window with $\langle L\rangle=70\hbar$ may be reached (see inset in Fig. 2). This value is well inside the composite system formation range (from zero to about $100\hbar$) predicted by the model.

Unfortunately, M_{th} is correlated with the relative contribution of events in which two reactions occurred in the same beam burst. Figure 3 shows distribution of the total energy of charged particles measured, in this experiment, in consecutive events. For $M_{th}=10$ [Fig. 3(a)] these random events are represented only by a negligible high-energy tail. For $M_{th}=16$ [Fig. 3(b)] the situation is similar, but for $M_{th}=19$ [Fig. 3(c)] the number of randoms is of the order of 30% of true events.

To improve selection of NCC's we have used the linear momentum tensor that gives the shape of each multifragmentation event in the linear momentum space [18]. Following a suggestion of Lopez and Randrup [19] the event shape analysis in the sphericity (S), coplanarity (C) plane was used by Cebra *et al.* [20] and Barz *et al.* [21] in order to distinguish between the sequential and prompt multifragmentation in a reaction ^{40}Ar + ^{51}V, at incident energies from 35 to 85 MeV/nucleon. In our case, beside the multiplicity threshold we impose on events an additional condition using the S,C plane. For $(S,C)=(1,0)$ the momentum surface defined by the linear momentum tensor has a spherical shape, for $[(3/4),(\sqrt{3}/4)]$ it has a disc shape, and for (0,0) it is a rodlike object. In an infinite multiplicity approximation, events from central collisions are represented by the (1,0) point. For rather low multiplicities of our reaction they are smeared over quite a large region, but not the same as for the DIC reaction. In Fig. 4, the ratio of the number of the composite system decays (as predicted by the event generator) to the total number of events is presented in the S,C plane with the same condition as in Fig. 3(b). The box size in Fig. 4 is proportional to this ratio. The inset in Fig. 4 shows distribution of this ratio along the $(c,d)(1,0)$ path. As one can see, the composite system decays predominate in the right part of the picture. We propose therefore a filter that together with the $M_{th}=16$ condition permits only the events that are located inside the triangle $(a,b)(1,0)$, in Fig. 4. The angular momentum window of this filter, predicted by the event generator, is presented in Fig. 2. It has a shape similar to the high multiplicity filter alone with $M_{th}=19$, however it selects events not contaminated by random events where two reactions occurred in the same beam burst [Fig. 3(d)].

To check our filter we have investigated the distribution of velocities from measured events in a special plane: v_{par},v_{rel}. Here v_{par} is a c.m. velocity (for all $Z>1$ particles in an event) projected on the $\vec{v}_1$-$\vec{v}_2$ axis. For each event $\vec{v}_1$ and $\vec{v}_2$ denote the velocities of the heaviest detected frag-

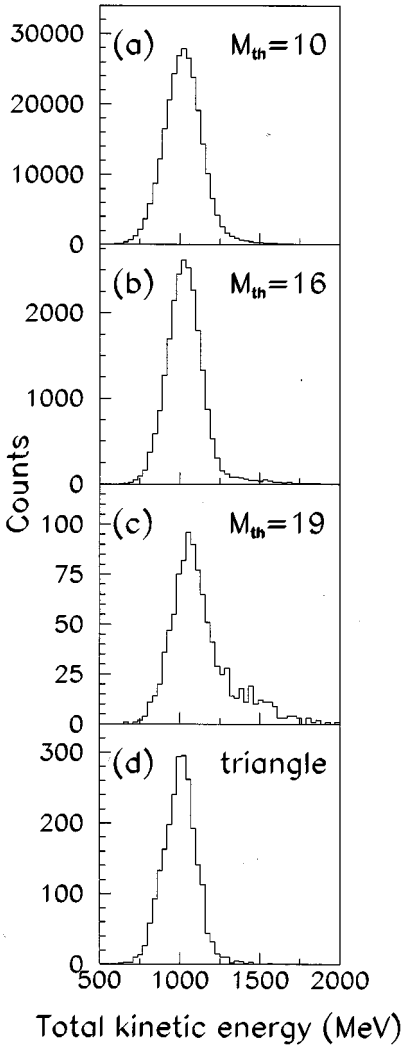

FIG. 3. Distribution of the total kinetic energy of charged particles measured event by event, for $33<Z_{tot}<41$ with (a) $M_{th}=10$, (b) $M_{th}=16$, (c) $M_{th}=19$, (d) $M_{th}=16$ plus restriction to events located inside the triangle $(a,b)(1,0)$ (Fig. 4).

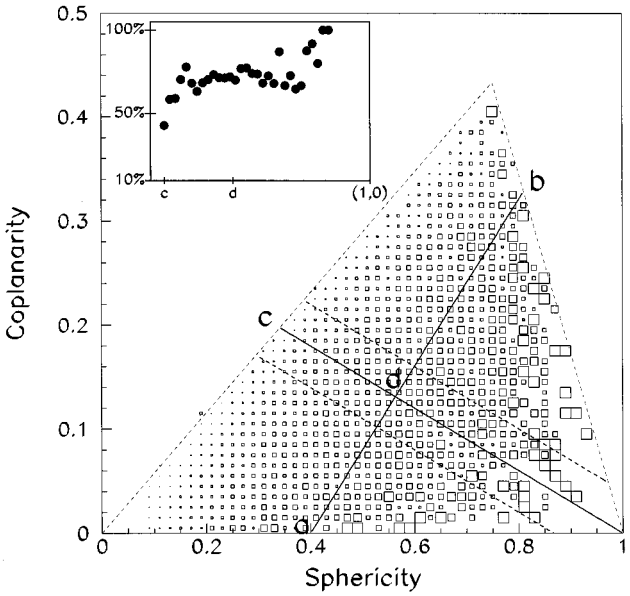

FIG. 4. Competition of NCC and DIC events (event generator) in the S,C plane given by $n_{NCC}/(n_{NCC}+n_{DIC})$, where n represents the corresponding number of cases. The inset shows distribution of this ratio along the $(c,d)(1,0)$ path. The width of the path is given by broken lines. The plot is prepared with conditions of Fig. 3(b).

ment and of the second heaviest, respectively. The relative velocity v_{rel} is defined here as $v_{rel}=|\vec{v}_1-\vec{v}_2|$. For DIC, v_{rel} depends on the energy dissipation (impact parameter) of a collision and for NCC on the potential barrier of the composite system. For the symmetric $^{40}Ca + {}^{40}Ca$ reaction the velocity vectors should be concentrated in two locations for a DIC collision, but only in one location for the light particle (LP) and IMF decay of a composite system.

As a first step we apply the low multiplicity filter $M<10$, which should select more peripheral collisions. Two hills [contour plot in Fig. 5(a)] with peaks located at v_{rel} of about 0.2c are seen in this case (c denotes the velocity of light). They can be identified as two hot Ca-like fragments moving apart with relative velocities $v_{rel}=|\vec{v}_1-\vec{v}_2|$. Because of anisotropy of energy thresholds and the granularity of AMPHORA the picture is not exactly symmetric around the zero point of the v_{par} axis. For the high multiplicity filter $M_{th}=10$ alone [Fig. 5(b)] a shoulder appears connecting the point located near the c.m. and having v_{rel} values of about 0.12c, with one of the DIC hills. It may represent composite Ca+Ca systems. For high multiplicities ($M_{th}=10$) slower-moving heavier DIC partners are discriminated by the detection system and therefore relative intensity of the source with v_{rel} of about 0.1c is artificially enhanced. Also one can observe that the left DIC peak is higher than the right one. It is so because a smaller number of emitted particles accompany the heaviest fragment (located at the right side). Figure 5(c) presents the situation in the v_{par},v_{rel} plane for the new filter which together with the $M_{th}=16$ condition permits these events only which are located inside the triangle $(a,b)(1,0)$ in Fig. 4. Now only one hill appears, located at the c.m. suggesting emission of particles from a composite system created in NCC's.

In order to visualize reaction scenarios of Fig. 5 in a different way, we propose to look at the angular distribution, $dN(\theta)/d\Omega$, of charged particles defined in the c.m. reference frame with the Z axis parallel to the vector $\vec{v}_{rel}$ defined as before. Here θ is the polar angle. For events from DIC's, the projectilelike fragment and the targetlike fragment decay by emission of LP and IMF's, and in the c.m. velocity space one should observe two bundles of velocity vectors, contained inside two cones, oriented along $\vec{v}_1$ and $\vec{v}_2$, respectively. The velocity vectors should therefore exhibit an angular distribution with maxima in directions of $\vec{v}_1$ and $\vec{v}_2$. In this case, $dN(\theta)/d\Omega$ should have a concave shape, with maxima in the vicinity of 0 and 180 degrees.

For a NCC collision after prompt multifragmentation, fragments belonging to some partition are accelerated along respective Coulomb trajectories. The two heaviest fragments of the partition (event) are emitted almost back to back [15,19]. At the beginning they create an axial, very strong Coulomb field that focuses the remaining charged ejectiles, giving a maximum in the $dN(\theta)/d\Omega$ distribution, located

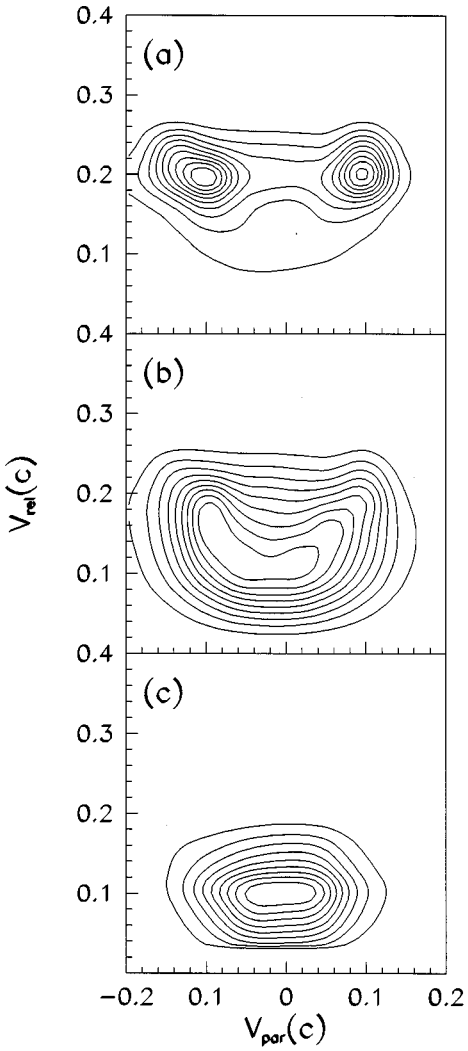

FIG. 5. Distribution of measured velocities of $Z>1$ particles in the v_{par}, v_{rel} plane (linear contour plot), for $33<Z_{tot}<41$. (a): for multiplicities <10 (b): for multiplicities $\geqslant 10$; (c): for multiplicities $\geqslant 16$ plus restriction to events located inside the triangle $(a,b)(1,0)$ (Fig. 4).

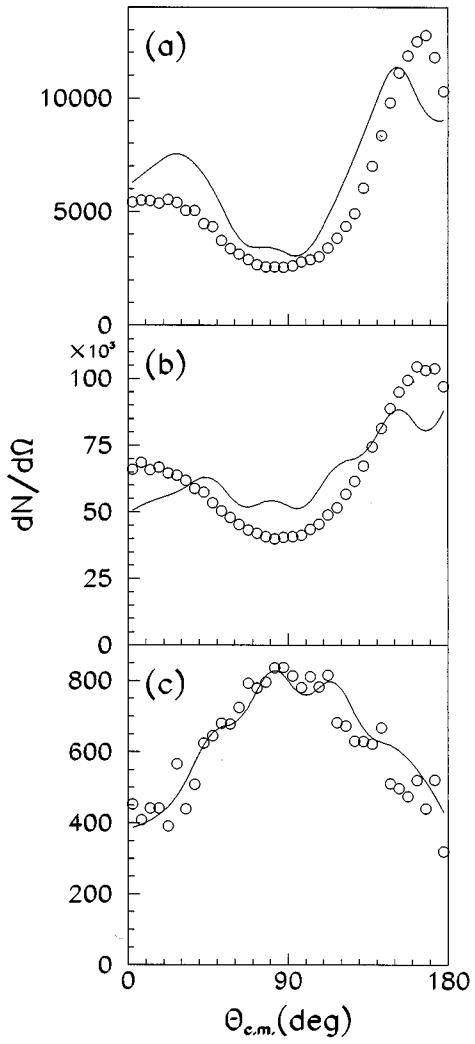

FIG. 6. The $dN(\theta)/d\Omega$ angular distribution for $33<Z_{tot}<41$. Additional conditions in 6(a)–6(c) are the same as in 5(a)–5(c). Solid lines represent predictions of the Monte Carlo event generator.

close to 90 degrees (see [15]). In the case of sequential multifragmentation one also gets a maximum in the $dN(\theta)/d\Omega$ distribution, although it is less pronounced [15]. Here also the two heaviest fragments are emitted almost back to back and, due to momentum conservation, other fragments are emitted preferentially in directions different from 0 and 180 degrees.

Figure 6 presents the $dN(\theta)/d\Omega$ distributions of $Z>1$ particles for the same filters as in Fig. 5. As seen from Fig. 6(a), the $dN(\theta)/d\Omega$ distribution has a concave shape as predicted for a DIC reaction. For $M_{th}=10$ [Fig. 6(b)] we still have a concave angular distribution suggesting a quite large admixture of the DIC events. However a relative minimum in the $dN(\theta)/d\Omega$ distribution is here shallower. The situation changes qualitatively when $M_{th}=16$ and the additional condition is imposed in the S,C plane. As seen in Fig. 6(c) the $dN(\theta)/d\Omega$ angular distribution has now a convex shape in agreement with our expectation for nearly central collisions.

In conclusion, we have investigated the ^{40}Ca + ^{40}Ca reaction at 35 MeV/nucleon using an improved configuration of the AMPHORA multidetector. Our results highlight the difficulties associated with separation of central collisions from DIC events in reactions of light symmetric ions. We have shown that together with the multiplicity and total charge thresholds the use of an additional condition in the S,C plane greatly improves the rejection of DIC events. Global variables S and C employed in the proposed filter make use of all detected products and are therefore well suited for sorting small impact parameters [10]. The proposed filter reduces the number of transmitted events to about 1/100 of the initial value, with the total charge threshold alone. This reduction factor is similar to that of the filter with $33<Z_{tot}<41$, and $M_{th}=19$ (predicted by the event generator) which creates a similar angular momentum window. However the total energy spectra (Fig. 3) strongly suggest that in our experiment the high multiplicity threshold alone cannot be used because of random events.

We have also proposed two representations of events use-

ful for monitoring contributions from the DIC sources. The first of them is the $v_{\mathrm{par}}, v_{\mathrm{rel}}$ map, where a DIC contribution appears as two hills. The second one is the charged-particle angular distribution, measured in a coordinate system oriented by the velocities of two heaviest fragments. The distribution changes shape from a concave to a convex curve, when the reaction scenario changes from DIC to a formation of a single composite system, which decays by emission of LP's and/or IMF's.

The authors are indebted to the SARA cyclotron staff for providing the excellent beam. This work was supported by the Polish-French (IN_2P_3) agreement and the Committee of Scientific Research of Poland, KBN Grant No. PB719/P3/93/04.

[1] K. Hagel *et al.*, Phys. Rev. C **50**, 2017 (1994), and references therein.
[2] See, e.g., J. Randrup and S. E. Koonin, Nucl. Phys. **A356**, 223 (1981); J. Bondorf, R. Donangelo, I. N. Mishustin, and H. Schulz, *ibid.* **A444**, 460 (1985); D. H. E. Gross, Rep. Prog. Phys. **53**, 605 (1990).
[3] W. A. Friedman, Phys. Rev. C **42**, 667 (1990).
[4] B. Borderie, Ann. Phys. (Paris) **17**, 349 (1992); D. R. Bowman *et al.*, Phys. Rev. Lett. **70**, 3534 (1993); O. Lopez *et al.*, Phys. Lett. B **315**, 34 (1993); M. Louvel *et al.*, *ibid.* **320**, 221 (1994).
[5] B. Borderie *et al.*, Phys. Lett. B **205**, 26 (1988); D. Jouan *et al.*, Z. Phys. A **340**, 63 (1991); M. Aboufirassi *et al.*, Report No. LPCC 93-14; A. Kerambrun *et al.*, Report No. LPCC 94-14; S. P. Baldwin *et al.*, Phys. Rev. Lett. **74**, 1299 (1995); J. Peter *et al.*, Nucl. Phys. **A593**, 95 (1995).
[6] Z. Sosin *et al.*, Nucl. Phys. **A574**, 474 (1994).
[7] C. Cavata *et al.*, Phys. Rev. C **42**, 1760 (1990); Y. D. Kim *et al.*, *ibid.* **45**, 338 (1992).
[8] T. Li *et al.*, Phys. Rev. Lett. **70**, 1924 (1993).
[9] C. A. Ogilvie *et al.*, Phys. Rev. C **40**, 654 (1989).
[10] J. Peter *et al.*, Nucl. Phys. **A519**, 611 (1990).
[11] D. Heuer *et al.*, Phys. Rev. C **50**, 1943 (1994).
[12] D. Drain *et al.*, Nucl. Instrum. Methods A **281**, 528 (1989).
[13] T. Barczyk *et al.*, Nucl. Instrum. Methods A **364**, 311 (1995).
[14] Z. Sosin and A. Wieloch (unpublished).
[15] W. Gawlikowicz and K. Grotowski, Acta Phys. Pol. **22**, 885 (1991); Nucl. Phys. **A551**, 73 (1993).
[16] Z. Sosin *et al.*, Acta Phys. Pol. **B25**, 1601 (1994).
[17] See the SIR code, D. Heuer *et al.* (unpublished).
[18] J. Cugnon *et al.*, Phys. Lett. **109B**, 167 (1982); M. Gyulassy *et al.*, *ibid.* **110B**, 185 (1982); G. Fai and J. Randrup, Nucl. Phys. **A404**, 551 (1983).
[19] J. A. Lopez and J. Randrup, Nucl. Phys. **A491**, 477 (1989).
[20] D. A. Cebra *et al.*, Phys. Rev. Lett. **64**, 2246 (1990).
[21] H. W. Barz *et al.*, Phys. Lett. B **267**, 317 (1991).